Journal of Catalysis **188,** 270–280 (1999)
Article ID jcat.1999.2644, available online at http://www.idealibrary.com on IDEAL®

CO and NO Adsorption on Alumina–Pd–Mo Catalysts: Effect of the Precursor Salts

F. B. Noronha,[1] M. A. S. Baldanza, and M. Schmal[2]

NUCAT-PEQ-COPPE, Universidade Federal do Rio de Janeiro, Ilha do Fundão, C.P. 68502, CEP 21941, Rio de Janeiro, Brazil

Received March 9, 1999; revised July 13, 1999; accepted July 13, 1999

The effect of the palladium precursor on the CO and NO adsorption capacity of Pd–MoO_3/Al_2O_3 catalysts was studied. TPR and IR analysis showed that the palladium addition promoted the reduction of Mo^{6+} to Mo^{4+}. The presence of a higher amount of molybdenum oxide partially reduced improved the NO dissociation to N_2 and N_2O on Pd–Mo/Al_2O_3 catalysts. This behavior was attributed to the formation of a lower fraction of inactive adsorbed nitrogen species on molybdenum oxide partially reduced. The catalytic behavior of the Pd–Mo/Al_2O_3 catalysts on the NO + CO reaction could be explained by a bifunctional mechanism. After adsorption and dissociation of NO on Mo^{4+}, the oxygen dissociated is transferred to the Pd. The CO adsorbed on the Pd surface reacts to CO_2.

Key Words: **Pd–Mo catalysts; CO + NO reaction; TPD of CO or NO; reaction mechanisms.**

INTRODUCTION

The three-way catalyst contains rhodium, platinum, or palladium. Rhodium is used as the active component for the selective reduction of nitric oxide to nitrogen with low-ammonia formation, even under slightly oxidizing conditions (1, 2). Recently, several studies have been performed to replace Rh in automotive catalysts in view of its high cost and scarce resources (3–7). Pd catalysts have not only a poor NO_x conversion but also a high-ammonia formation under rich conditions (1). However, it was reported that the addition of MoO_3 to Pd/Al_2O_3 catalysts improved the NO activity with high selectivity to N_2 in the presence of a small excess of oxygen (4, 6, 7). It is important to stress that Pd–Mo/Al_2O_3 catalysts have been used to control the exhaust emissions of ethanol-fueled Brazilian vehicles (8).

According to Gandhi *et al.* (4), the high selectivity for the NO reduction is due to Pd–Mo interactions. Based on TPR and IR analyses, they ascribed these results to the presence of a surface Pt^0–Mo^{4+} complex that had activity and selectivity behavior similar to that observed on rhodium catalysts.

To better understand the Pd–Mo interaction, Halasz *et al.* (5) studied the preparation method of the Pd–Mo catalysts by DRX and TPR. They used different salts ($(NH_4)_2MoO_4$, $Mo(CO)_6$, $PdCl_2$, and $Pd(NH_3)_4Cl_2$) and impregnation methods (coimpregnation or successive impregnation). A close proximity between the metals was obtained on the catalysts prepared by impregnation of Mo/Al_2O_3 ($(NH_4)_2MoO_4$) with $Pd(NH_3)_4Cl_2$. In the case of the catalysts prepared by impregnation of Mo/Al_2O_3 ($(NH_4)_2MoO_4$) with $PdCl_2$, a high amount of molybdenum was necessary to completely cover the surface of alumina and to assure an intimate contact between both metals. The catalytic activity and selectivity of the latter catalyst for reduction of nitric oxide by carbon monoxide and by hydrogen in the presence of different amounts of oxygen was also performed (6). The catalyst containing 2% Pd and 20% Mo had not only activity slightly higher than the commercial Pt–Rh catalyst but also high selectivity for nitrogen and nitrous oxide under oxidizing conditions. According to them, the carbon monoxide affects the reduction of nitric oxide.

Aiming to improve the contact between the molybdenum oxide and the noble metal, Hoost *et al.* (7) prepared a MgO-supported Pd–Mo catalyst from an organometallic precursor that had both metals chemically bound together. In spite of the low Mo content (1 wt% Mo), the catalyst made from the bimetallic precursor showed higher selectivity than a Pd–Mo catalyst prepared from monometallic precursors. These results were attributed to Pd–Mo interactions that were stronger on the catalyst based on the bimetallic precursor.

Therefore, it is established that a high selectivity toward nitrogen on Pd–Mo catalysts is due to the interaction between both metals. However, it is not clear how the molybdenum oxide affects the adsorptive properties of the noble metal to explain the catalytic behavior of these systems.

The aim of this work is to study the effect of the palladium precursor on the CO and NO adsorption capacity of

[1] Present address: Instituto Nacional de Tecnologia (INT), Av. Venezuela 82, CEP 20081-310, Rio de Janeiro, Brazil. Fax: (55-21) 2636552. E-mail: bellot@peq.coppe.ufrj.br.

[2] To whom correspondence should be addressed. Fax: (55-21) 2906626. E-mail: schmal@peq.coppe.ufrj.br.

0021-9517/99 $30.00

$Pd–MoO_3/Al_2O_3$ catalysts to better understand the CO + NO reaction mechanism on these catalysts.

EXPERIMENTAL

Catalyst Preparation

An $8\%Mo/Al_2O_3$ catalyst was prepared by Al_2O_3 (Engelhard; BET area = 189 m^2/g) impregnation with an aqueous solution of $(NH_4)_6 \cdot Mo_7O_{24} \cdot 4H_2O$. The sample was dried at 383 K for 22 h and calcined under air flow at 773 K for 2 h. Pd/Al_2O_3 and $Pd–Mo/Al_2O_3$ samples were obtained by impregnation of Al_2O_3 and Mo/Al_2O_3, respectively, with a solution of palladium precursor. Two salts were used: $PdCl_2$ and $Pd(NO_3)_2$ (Aldrich). Then, the samples were dried at 383 K, followed by calcination under air flow at 773 K for 2 h. The prepared catalysts, their nomenclature, and their composition are presented in Table 1.

Catalyst Characterization

Diffuse reflectance spectroscopy (DRS). Diffuse reflectance spectra were recorded in the range of 200–900 nm using an UV–vis NIR spectrophotometer (Cary 5E-Varian) equipped with an integrating sphere (Harrick). The support (pure alumina) and $8\%Mo/Al_2O_3$ sample were used as reference for the Pd/Al_2O_3 and $Pd–Mo/Al_2O_3$ samples, respectively.

Temperature-programmed reduction (TPR). TPR experiments were performed in a conventional apparatus, as described previously (9). Before reduction, the catalysts were heated at 423 K in flowing argon for 0.5 h. Then, a mixture of 1.6% hydrogen in argon flow was passed through the sample and the temperature was raised at 8 K/min from 298 up to 1223 K.

H_2 and CO chemisorption. The chemisorption uptakes were measured in an ASAP 2000C (Micromeritics) apparatus. Before reduction, the catalysts were dehydrated at 423 K for 0.5 h. Then, the catalysts were reduced at 773 K (5 K/min) in flowing H_2 (30 cm^3/min). Following reduction, the samples were evacuated for 1 h at the reduction temperature and cooled to the adsorption temperature under vacuum. Irreversible uptakes were determined from dual isotherms measured for hydrogen (at 343 K) and carbon monoxide (at 298 K) using the method of Benson *et al.* (10).

TABLE 1

Catalyst Composition

Catalyst	Palladium precursor salt	Pd (wt%)	Mo (wt%)
Mo/Al_2O_3	—	—	7.50
Pd/Al_2O_3 (Cl)	Chloride	1.25	—
Pd/Al_2O_3 (N)	Nitrate	0.97	—
$Pd–Mo/Al_2O_3$ (Cl)	Chloride	1.02	7.74
$Pd–Mo/Al_2O_3$ (N)	Nitrate	0.90	7.49

TABLE 2

Major Fragments of Products Desorbed during CO or NO TPD and Intensity Ratios of Mass Fragments

Products	Major fragments	Intensity ratios for mass fragments
CO	28	—
CO_2	44, 28	44/28 = 9.96
N_2	28	—
NO	30	—
N_2O	44, 30, 28	44/28 = 7.80 44/30 = 2.94

Infrared spectroscopy of adsorbed carbon monoxide or nitrogen monoxide. CO or NO adsorption was followed by Fourier transform infrared spectrometer (Perkin-Elmer 2000). The samples were evacuated at 423 K for 1 h and then reduced at 773 K for 1 h. After vacuum outgassing at the reduction temperature for 1 h, the catalyst was cooled to room temperature. Afterward, either 30 Torr (1 Torr = 133.3 N/m^2) of CO or 7 Torr of NO was introduced. Following adsorption, the catalysts were outgassed at 298 K for 1 h and the IR spectrum was obtained at room temperature (resolution of 2 cm^{-1}).

CO and NO temperature-programmed desorption (TPD). TPD of adsorbed CO or NO was carried out in a microreactor coupled to a quadrupole mass spectrometer (Prisma, Balzers). A Quadstar analytical system was used to select a series of masses and record the signal intensity for each mass as a function of temperature. The procedure was similar for all experiments. At first, the catalysts were purged under helium flow (50 cm^3/min) at a heating rate of 10 K/min from room temperature up to 823 K. Then, the catalysts were cooled to room temperature and reduced at 773 K for 1 h, in a flow of pure H_2 (30 cm^3/min). Following reduction, the microreactor was outgassed with helium at the reduction temperature for 0.5 h and cooled to room temperature. The adsorption of CO was performed by passage of pulses of a mixture of 5% CO in helium. The same procedure was taken for NO but a mixture of 1% NO in helium was used. After adsorption, the catalysts were heated at 20 K/min up to 823 K in flowing helium at 50 cm^3/min. The mass spectrometer was calibrated with helium mixtures containing specified concentrations of CO, NO, or N_2O or pure CO_2, H_2, N_2, and Ar. The fragmentation pattern of the products were experimentally determinated through their introduction into the mass spectrometer separately. The values obtained are presented in Table 2. The distribution of desorbed products was calculated from the TPD spectra of individual mass fragments as follows. From the most intense fragment of each product, the

corresponding amounts of their other fragments were determined, taking into account the ratios of intensity of the mass fragments. In the case of carbon dioxide ($m/e = 44$), the secondary fragment was $m/e = 28$. Then, after subtraction of the contributions from carbon dioxide, the signal $m/e = 28$ obtained was assigned to carbon monoxide. The same procedure was applied to the desorption spectra of compounds containing nitrogen atoms. The distribution of desorbed products was based on the number of desorbed moles of CO and CO_2 or N_2, N_2O, and NO.

Catalytic activity. The catalytic experiments were performed in a microreactor at atmospheric pressure. Catalysts (ca. 100 mg) were pretreated in helium (ml/min) at 823 K for 1 h. The reaction mixture that consisted of 1.0% CO/0.6% NO was balanced with He flow (150 ml/min; space velocity = 100,000 h^{-1}). The effluent products were analyzed by online gas chromatography using a TCD detector and a Carbosieve Carboxen 1000 column with Cryogen.

RESULTS AND DISCUSSION

Precursor State and Pd–Mo Interaction

The DRS spectra of Pd/Al_2O_3 and $Pd–Mo/Al_2O_3$ are presented in Fig. 1. The spectrum of the Pd/Al_2O_3 (Cl) sample exhibited three bands at 286, 325, and 460 nm (Fig. 1a). According to the literature, the band at 286 nm is ascribed to a metal–ligand charge transfer (11). The band located around 325 nm arises from the $Pd(H_2O)_4^{2+}$ complex since the measurements were performed in contact with air. The band at 460 nm is attributed to a *d–d* transition. On the other hand, the spectrum of the Pd/Al_2O_3 (N) sample showed bands at 334 and 466 nm, corresponding to the $Pd(H_2O)_4^{2+}$ complex and the *d–d* transition, respectively (Fig. 1b).

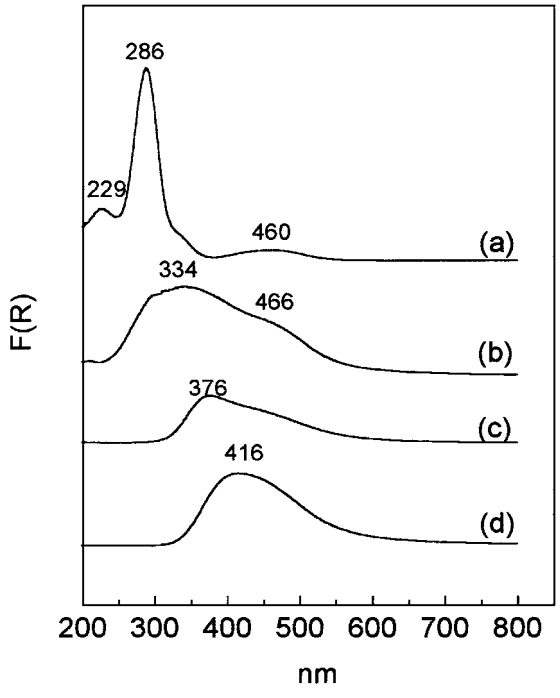

FIG. 1. DRS spectra of $Pd–Mo/Al_2O_3$ catalysts: (a) Pd/Al_2O_3 (Cl); (b) Pd/Al_2O_3 (N); (c) $Pd–Mo/Al_2O_3$ (Cl); (d) $Pd–Mo/Al_2O_3$ (N).

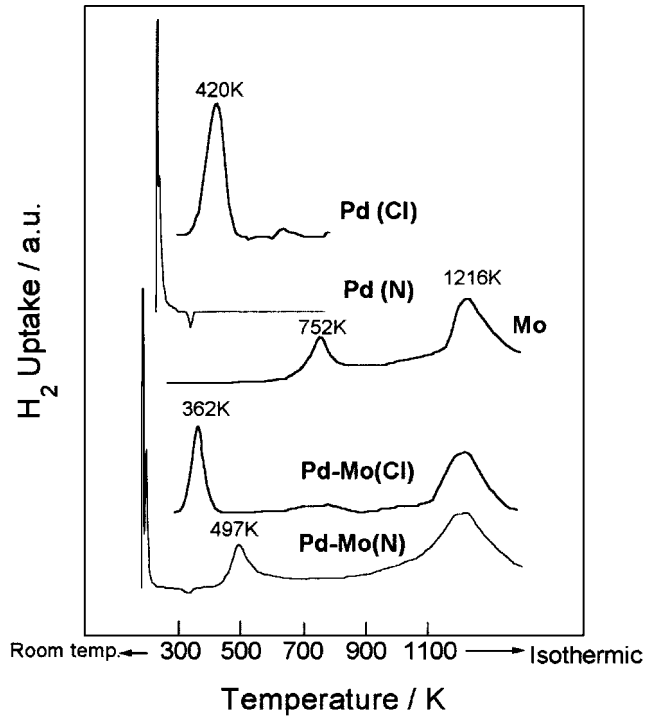

FIG. 2. TPR profile of $Pd–Mo/Al_2O_3$ catalysts.

Rakai *et al.* (11) compared the diffuse reflectance spectra of bulk PdO with those of alumina-supported Pd samples prepared from chloride and nitrate precursors. On the Pd/Al_2O_3 (Cl), the charge transfer band at 280 nm was attributed to the presence of chloride ions in the coordination sphere of Pd^{2+} ions which suggests the formation of oxychloride species during calcination in air. Pd/Al_2O_3 (N) presented only a broad peak near 380 nm which was ascribed to PdO particles. Our results are in good agreement with those obtained by Rakai *et al.* (11).

The spectrum of the $Pd–Mo/Al_2O_3$ (Cl) sample displayed a band at 376 nm and a shoulder at 450 nm (Fig. 1c). However, the MoO_3 addition led to the disappearance of the band assigned to charge transfer. These results suggested that the monolayer surface coverage of the alumina was attained and PdO was the main species. In fact, IR spectroscopy showed that the surface hydroxyls completely disappeared on the $8\% Mo/Al_2O_3$ sample, which confirmed the formation of a monolayer surface coverage at this molybdenum oxide concentration. The $Pd–Mo/Al_2O_3$ (N) sample presented only a single broad band around 416 nm, corresponding to PdO particles (Fig. 1d).

The TPR profile of Mo/Al_2O_3, Pd/Al_2O_3, and $Pd–Mo/Al_2O_3$ catalysts are shown in Fig. 2.

The TPR profile of the Mo/Al_2O_3 catalyst displayed two peaks at 752 and 1216 K. The lower temperature peak has been attributed to the reduction of Mo^{6+} to Mo^{4+} whereas the one at high temperature is due to the removal of oxygen atoms in the sublayer (12).

The Pd/Al_2O_3 (Cl) catalyst showed a peak at 420 K and a broad desorption peak between 600 and 800 K. On the other hand, the TPR profile of the Pd/Al_2O_3 (N) catalyst was totally different. In this case, a hydrogen consumption at room temperature was observed, followed by a negative peak around 337 K. In fact, the Pd oxychloride species are more strongly linked to the support than the PdO species, which explains the reduction at higher temperatures. Thus, the peak at 420 K was assigned to the reduction of PdO_xCl_y whereas the hydrogen consumption at room temperature corresponded to the reduction of PdO. These results are in good agreement with the DRS analysis. The negative peak observed on Pd/Al_2O_3 (N) has been reported as the desorption of weakly adsorbed hydrogen from the palladium surface and the decomposition of palladium hydride formed at room temperature (9, 13, 14).

The $Pd–Mo/Al_2O_3$ (Cl) catalyst displayed three hydrogen uptakes at 362, 774, and 1216 K. The hydrogen uptake at 362 K indicated that not only was PdO reduced but also Mo^{6+} to Mo^{4+} reduction occurred (Table 3). The palladium addition strongly promoted the molybdenum oxide reduction, as seen by the decrease of the hydrogen uptake at 774 K. However, the removal of the oxygen atom in the sublayer (1216 K) was not influenced by the presence of palladium.

The TPR profile of the $Pd–Mo/Al_2O_3$ (N) catalyst exhibited three peaks: at room temperature, 497 K, and 1216 K. In this case, the promoting effect of palladium was more evidenced since the reduction of molybdenum oxide at room temperature was observed (Table 3). Furthermore, the palladium addition shifted the position of the peak corresponding to Mo^{6+} to Mo^{4+} reduction toward lower temperature (497 K). As was seen for the $Pd–Mo/Al_2O_3$ (Cl) catalyst, palladium did not catalyze the removal of oxygen atoms in the sublayer.

TABLE 3

Hydrogen Consumption during TPR

Samples	H_2 consumption (μmol of H_2/g_{cat})			
	298 K[a]	298–450 K	450–900 K	900–1223 K
Mo/Al_2O_3	—	143	894	1018
Pd/Al_2O_3 (Cl)	—	73	—	—
Pd/Al_2O_3 (N)	90	—	—	—
$Pd–Mo/Al_2O_3$ (Cl)	—	359	265	542
$Pd–Mo/Al_2O_3$ (N)	233	384	780	899

[a] Hydrogen consumption at room temperature.

TABLE 4

Hydrogen Adsorption, Palladium Dispersion, and H_2/CO Ratio Obtained from Chemisorption

Catalyst	Consumption (μmol/g_{cat})		Dispersion (%)		H_2/CO ratio
	H_2	CO	H_2	CO	
Mo/Al_2O_3	0.13	0.87	—	—	0.2
Pd/Al_2O_3 (Cl)	20.9	29.3	45	31	0.7
Pd/Al_2O_3 (N)	3.01	4.73	6	5	0.6
$Pd–Mo/Al_2O_3$ (Cl)	4.3	20.3	9	22	0.2
$Pd–Mo/Al_2O_3$ (N)	1.23	14.2	3	15	0.1

TPR analysis of $Pt–MoO_3/Al_2O_3$ catalysts indicated that the presence of the noble metal lowers the temperature for the removal of capping oxygen of MoO_3 but it does not significantly affect the peak around 1200 K (4, 15). These results were attributed to the interaction between the noble metal and molybdenum oxide with the formation of a stable complex with Pt atoms and the partially reduced Mo ions.

The palladium addition mainly promoted the reduction of Mo^{6+} to Mo^{4+}, in agreement with the literature (4, 15–17), which suggests the existence of a strong interaction between Pd^0 and Mo oxide. However, the $Pd–Mo/Al_2O_3$ catalyst prepared from a nitrate precursor seemed to have a stronger interaction between them. It could be explained by the presence of a higher amount of PdO, which is easily reduced, even at room temperature.

The Effect of MoO_3 Addition on H_2, CO, and NO Adsorption Properties of Pd

The amount of H_2 and CO irreversibly adsorbed on the Pd/Al_2O_3 and $Pd–Mo/Al_2O_3$ catalysts and the dispersion values are presented in Table 4.

At first, it is important to stress that hydrogen was not irreversibly adsorbed on the Mo/Al_2O_3 catalyst whereas CO adsorption was observed on this catalyst. In fact, the infrared spectra of CO adsorbed on the Mo/Al_2O_3 catalyst showed a band at 2191 cm^{-1} (Fig. 3b). According to the literature, this band has been attributed to CO chemisorption on partially reduced molybdenum oxide (4).

The dispersion of the Pd/Al_2O_3 (Cl) catalyst was 45% while the Pd/Al_2O_3 (N) catalyst showed a very low dispersion (6%). As suggested by Rakai *et al.* (11), the palladium oxychloride species present on Pd/Al_2O_3 (Cl) should be strongly attached to the support surface, resulting in a high metal dispersion. Since PdO was the main species on the Pd/Al_2O_3 (N) sample, a lower dispersion was expected.

In spite of the great difference of dispersion between Pd/Al_2O_3 (Cl) and Pd/Al_2O_3 (N) catalysts, the H_2/CO ratio was approximately the same.

The infrared spectrum of the irreversibly adsorbed carbon monoxide on Pd/Al_2O_3 (Cl) displayed two absorption

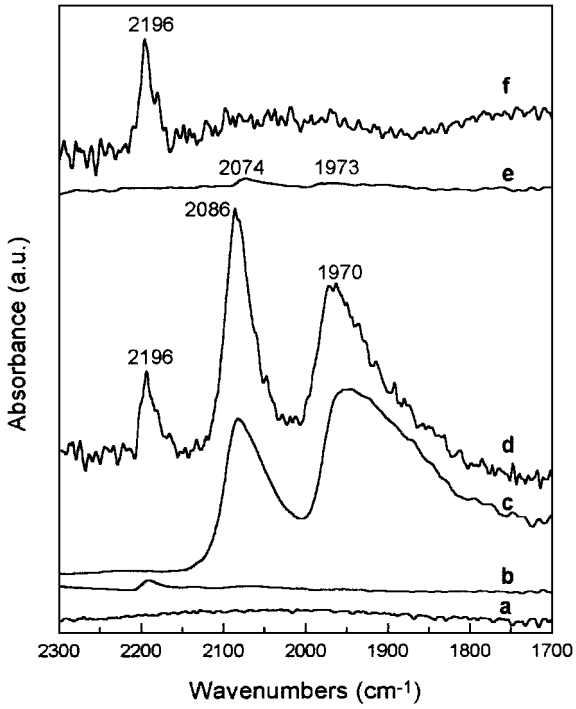

FIG. 3. Infrared spectra of CO adsorbed on (a) Al_2O_3, (b) Mo/Al_2O_3, (c) Pd/Al_2O_3 (Cl), (d) $Pd–Mo/Al_2O_3$ (Cl), (e) Pd/Al_2O_3 (N), and (f) $Pd–Mo/Al_2O_3$ (N).

bands at 1945 and 2082 cm^{-1} (Fig. 3c). In the literature (18, 19), these bands correspond to carbon monoxide bonded to palladium atoms in bridge and linear forms, respectively. The Pd/Al_2O_3 (N) catalyst also exhibited two bands around 2074 and 1973 cm^{-1} (Fig. 3e), which were weaker than the previous ones on the catalyst prepared from the chloride precursor. It was probably due to its lower dispersion.

The addition of molybdenum oxide decreased the hydrogen adsorption mainly on the catalyst based on the chloride precursor (Fig. 3d). The infrared spectrum of carbon monoxide adsorbed on palladium was similar to that on Pd/Al_2O_3 (Cl). A band above 2000 cm^{-1}, which was attributed to a linear adsorbed species, and another one below 2000 cm^{-1}, which corresponded to a bridged species, were observed. However, the relative intensities of these bands changed. The linear/bridged carbon monoxide ratio increased in the presence of MoO_3 . This behavior was also observed on alloys between metals of the VIII and Ib groups (20, 21). Then, these results were attributed to the dilution effect of Pd among MoO_3.

In the case of the $Pd–Mo/Al_2O_3$ (N) catalyst, the linear and bridged carbon monoxide bands completely disappeared, even after CO adsorption at room temperature (Fig. 3f). Therefore, it was not possible to attribute this result, either to the presence of a Pd–Mo interaction or to the low dispersion of this catalyst.

On the other hand, whatever the precursor salt, the Pd–Mo catalysts showed a band around 2196 cm^{-1}, which corresponds to the CO adsorption on partially reduced molybdenum oxide. This result could explain the increase of the amount of chemisorbed CO on the Pd–Mo catalysts, as shown by the strong decrease of the H_2/CO ratio (Table 4). Furthermore, in comparison with the IR spectra of CO adsorbed on Mo/Al_2O_3, the intensity of the band at 2190 cm^{-1} increased in the presence of palladium. It was assigned to the higher amount of partially reduced molybdenum oxide on the Pd–Mo catalysts, as revealed by TPR. These results confirmed the existence of a palladium–molybdenum oxide interaction.

The increase of the desorption temperature led to a decrease of the intensity of the band around 1940 and 2080 cm^{-1} (Fig. 4). However, the intensity band around 2080 cm^{-1} decreased much more than that of the band around 1940 cm^{-1}. Therefore, these results indicate that the linearly bonded CO is more weakly adsorbed than the bridge-bonded CO. After desorption at 373 K, both adsorption forms decreased but this effect was more pronounced on the Pd–Mo (Cl) catalyst, disappearing then completely. It seems that MoO_3 weakened the adsorption strengths of carbon monoxide on palladium. The same trend was observed by Hicks *et al.* (22) through IR studies of CO adsorption on Pd/La_2O_3. The decrease of the carbon monoxide adsorption strength was attributed to a weakening in the σ-bond component of the Pd–CO bond due to a charge

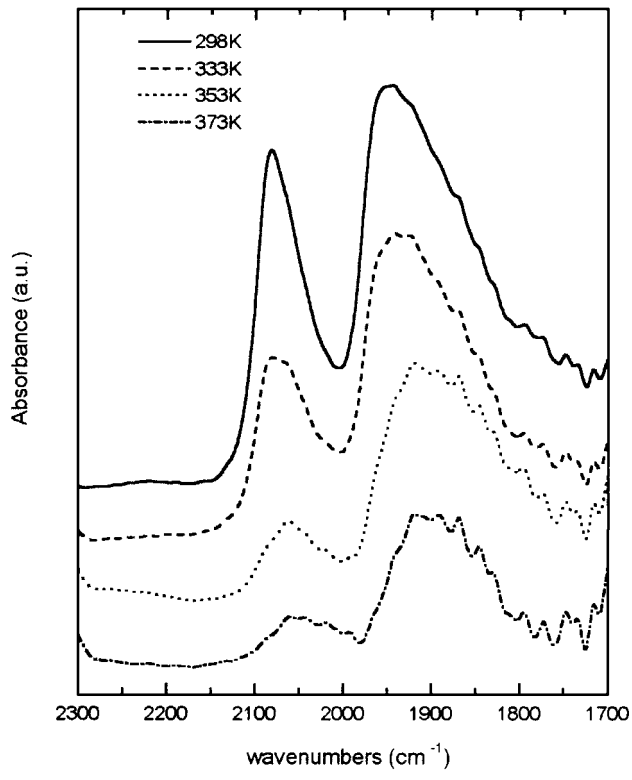

FIG. 4. Infrared spectra of CO adsorbed on Pd/Al_2O_3 (Cl) after evacuation at different temperatures.

transfer from LaO_x patches to Pd particles. It suggests the formation of new adsorption sites in the presence of molybdenum oxide partially reduced.

The TPD profile for CO desorption from the Mo/Al_2O_3 catalyst showed only one small peak around 400 K. The formation of CO_2 was not observed.

The TPD curves following carbon monoxide adsorption on the Pd/Al_2O_3 (Cl) catalyst displayed four peaks at 377, 470, 613, and 823 K (Fig. 5a). These peaks were in good agreement with those reported previously for Pd/SiO_2 (23–25). By comparing the CO TPD results (23) with the infrared spectra (22), Rieck and Bell attributed the two peaks at low temperatures in the TPD spectra to linearly bonded CO. The peaks at high temperature were assigned to bridge-bonded CO on Pd(100) and Pd(111) planes, respectively. Therefore, based on IR results, we could also assign the individual peaks in the TPD spectra to particular modes of CO adsorption. Since the linearly bonded CO was more weakly adsorbed than the bridge-bonded CO, we assigned the peaks at 377 and 470 K to linearly bonded CO, whereas

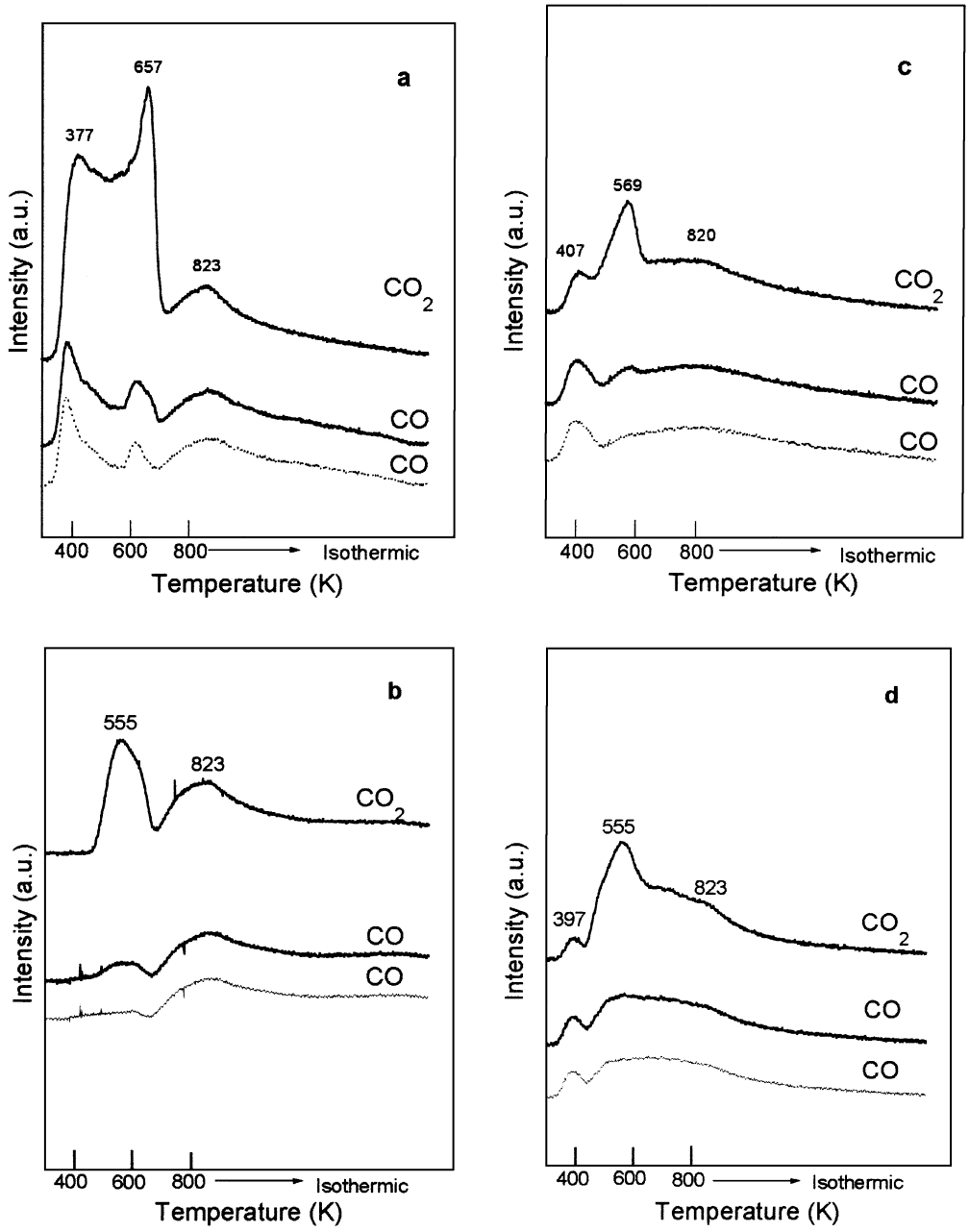

FIG. 5. TPD spectra of CO adsorbed on (a) Pd/Al_2O_3 (Cl), (b) Pd/Al_2O_3 (N), (c) $Pd–Mo/Al_2O_3$ (Cl), and (d) $Pd–Mo/Al_2O_3$ (N). Dashed lines correspond to corrected spectra.

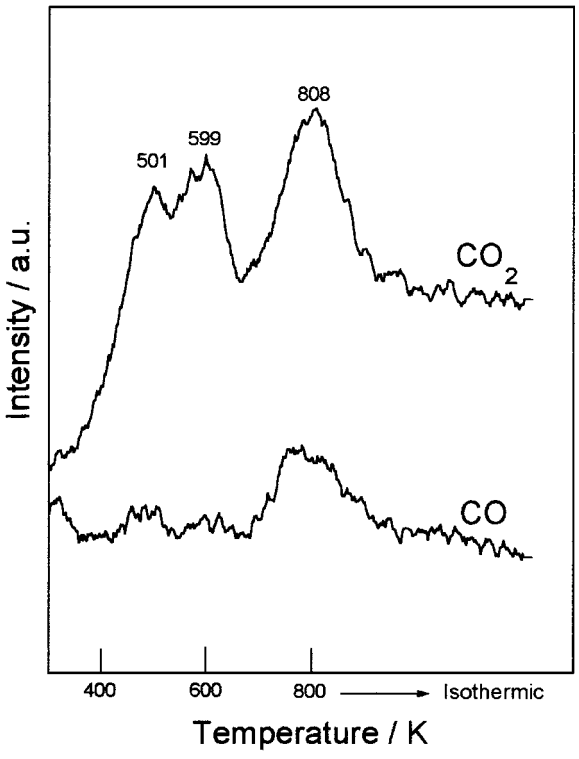

FIG. 6. TPO analysis after CO TPD on Pd/Al_2O_3 (Cl).

the two peaks at 613 and 823 K were attributed to bridge-bonded CO.

A significant amount of CO_2 was observed during the CO desorption. However, since no H_2 evolved with the CO_2 at 377 and 823 K, the formation of this CO_2 was attributed to the disproportionation of CO on the palladium surface, based on the stoichiometry $2CO_{ads} \rightarrow C_{ads} + CO_2$. Rieck and Bell (23, 25) also observed the appearance of CO_2 during CO TPD from Pd/SiO_2 catalysts, which was attributed to the disproportionation of CO on the palladium surface. The presence of carbonaceous species on the palladium surface was confirmed by TPO analysis after the TPD. Figure 6 shows the signal of $m/e = 28$ and 44 corresponding to CO and CO_2 formation during the TPO analysis. The CO_2 profile displayed three peaks at 501, 599, and 808 K and one peak was observed for CO around 800 K, which evidenced the carbon deposition on Pd as the result of the Bouduart reaction.

In addition to CO_2 a small amount of H_2 and H_2O was observed in the desorbing gas around 660 K. This indicates that the water–gas shift reaction of adsorbed CO with the hydroxyl of the support took place at this temperature range (Eqs. [1] and [2]) (26). Rieck and Bell (23–25) did not verify this result, probably due to the higher hydroxyl concentration on alumina compared to that on silica.

$$CO + 2OH^- \rightarrow CO_2 + H_2O, \quad [1]$$

$$CO + H_2O \rightarrow CO_2 + H_2. \quad [2]$$

The TPD profile of CO on the Pd/Al_2O_3 (N) catalyst exhibited only one peak at 823 K, which corresponds to the desorption of bridge-bonded CO on Pd (Fig. 5b). It can be seen that the amount of linearly bonded CO disappeared and the amount of bridge-bonded CO increased as the dispersion decreased. This trend agreed very well with the work of Rieck and Bell (25). In addition, two CO_2 peaks were observed at 555 and 823 K. The formation of H_2 around 600 K suggested the presence of the water–gas shift reaction, as noted on the Pd/Al_2O_3 (Cl) catalyst. The CO_2 peak at higher temperature was due to the disproportionation reaction of CO.

The TPD spectra of CO adsorbed on $Pd–Mo/Al_2O_3$ catalysts were very similar, whatever the precursor salt (Figs. 5c and 5d). This agreed well with the H_2 chemisorption results since both catalysts presented low dispersion. They exhibited two CO peaks around 400 and 560 K and a broad peak at 820 K. The first one was mainly due to desorption of CO adsorbed on molybdenum oxide partially reduced. The other two peaks were attributed to the linearly bonded and bridge-bonded CO on Pd. The addition of molybdenum oxide led to a preferential suppression of the bridged CO form on palladium, probably due to the dilution of palladium particles by MoO_x moieties. This behavior agreed well with the IR and TPD results of CO adsorption on Pd/La_2O_3 and lanthana-promoted Pd/SiO_2 catalysts (22, 23). Furthermore, the total amount of CO desorbed increased in the presence of molybdenum oxide (Table 5), which corresponds to CO desorption from the molybdenum oxide partially reduced. This was in good agreement with our previous results (27). It is important to note that TPR results revealed that the promoting effect of palladium on molybdenum oxide reduction was more important on the $Pd–Mo/Al_2O_3$ (N) catalyst. In spite of this, the $Pd–Mo/Al_2O_3$ (Cl) catalyst presented a higher amount of CO adsorbed (Table 4) and desorbed (Table 5). This result showed that metallic dispersion still plays an important role on Pd–Mo catalysts. The appearance of CO_2 was assigned to the dispropotionation of CO on the palladium surface, since H_2 desorption was not observed. This result was closely connected with a monolayer surface coverage of alumina and the disappearance of the surface hydroxyls.

TABLE 5

Yield (Carbon or Nitrogen Basis) of Products Desorbed during TPD of CO or NO

Catalyst	Yield (%)		Yield (%)		
	CO	CO_2	NO	N_2O	N_2
Pd/Al_2O_3 (Cl)	25	75	60	9	31
Pd/Al_2O_3 (N)	28	72	42	15	43
$Pd–Mo/Al_2O_3$ (Cl)	40	60	1	21	78
$Pd–Mo/Al_2O_3$ (N)	32	68	13	15	72

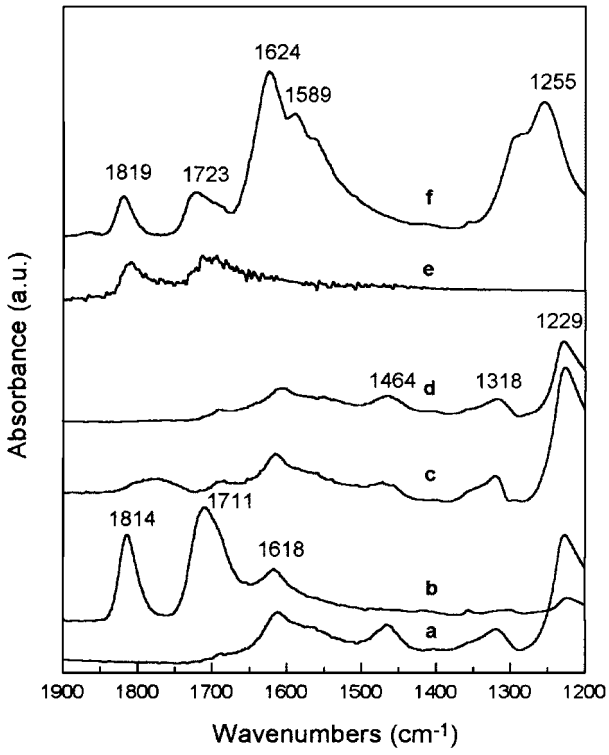

FIG. 7. Infrared spectra of NO adsorbed on (a) Al_2O_3, (b) Mo/Al_2O_3, (c) Pd/Al_2O_3 (Cl), (d) Pd/Al_2O_3 (N), (e) $Pd–Mo/Al_2O_3$ (Cl), and (f) $Pd–Mo/Al_2O_3$ (N).

Figure 7a shows the FTIR spectra of alumina after exposure to NO at room temperature, followed by evacuation at 298 K. The bands at 1228, 1320, 1467, 1562, and 1612 cm^{-1} have been reported for NO adsorption on alumina due to nitrate and nitrite complexes (28, 29).

The infrared spectra of NO adsorption on the $8\%Mo/Al_2O_3$ catalyst is presented in Fig. 7b. The addition of molybdenum led to a strong suppression of the bands attributed to the adsorption of NO on alumina. This suggested that molybdenum was well dispersed over the alumina surface. Furthermore, compared to NO adsorption on alumina, there are two new bands at 1814 and 1711 cm^{-1}. These bands were assigned to NO adsorption on partially reduced molybdenum species (27, 30).

The IR spectra of NO adsorption on the Pd/Al_2O_3 (Cl) catalyst showed basically the same bands present on pure alumina (Fig. 7c). However, a new broad band appeared around 1775 cm^{-1}. According to the literature, three NO adsorption bands on Pd/Al_2O_3 catalysts were reported around 1753–1750 cm^{-1} (linear), 1615–1599 cm^{-1} (two-fold bridged), and 1580–1572 cm^{-1} (three-fold bridged) (28). In this work, only the linear form of NO was observed, probably due to the superposition of the bridged NO band on reduced Pd by the NO adsorption bands on the support.

The Pd/Al_2O_3 (N) catalyst showed only the bands of NO adsorbed on alumina (Fig. 7d). Unlike the Pd/Al_2O_3 (Cl) catalyst, the linear adsorption mode for NO on Pd (1775 cm^{-1}) was absent.

The $Pd–Mo/Al_2O_3$ (Cl) catalyst exhibited only the bands corresponding to NO adsorption on molybdenum oxide partially reduced (1704 and 1811 cm^{-1}) (Fig. 7e). All the bands attributed to both NO adsorbed on alumina and palladium disappeared. Hoost *et al.* (28) reported a decrease of NO adsorption on the lanthana-promoted Pd/Al_2O_3 catalyst. According to them, this result was due to either a coverage of palladium particles by LaO_x patches or an increase in NO dissociation. On the $Pd–Mo/Al_2O_3$ (Cl) catalyst, the decrease of the hydrogen adsorption and the increase of the linear/bridged carbon monoxide ratio agreed well with the dilution or blocking of the palladium surface by molybdenum species. However, the increase of NO dissociation cannot be discarded.

Figure 7f displays the spectrum of NO adsorption on the $Pd–Mo/Al_2O_3$ (N) catalyst. The bands at 1723 and 1819 cm^{-1} correspond to the NO adsorption on molybdenum oxide partially reduced. However, unlike the Pd–Mo catalyst prepared from the chloride precursor, the bands associated to the NO adsorption on alumina increased drastically. In addition, these bands were shifted toward higher wavelengths (1255, 1589, and 1624 cm^{-1}) and a new one appeared at 1295 cm^{-1}. These resuts suggested that the impregnation of the calcined Mo/Al_2O_3 precursor with an acid solution of palladium nitrate affected the alumina surface.

The TPD spectra of adsorbed NO on Pd/Al_2O_3 (Cl) are shown in Fig. 8a. NO, N_2O, and N_2 were the nitrogen-containing products detected during the TPD. The NO profile exhibited a shoulder at 430 K and a narrow peak centered at 542 K. The N_2 spectrum displayed a single broad peak centered at 780 K. The N_2O signal consisted of a small peak at 540 K and a broad peak around 780 K.

The Pd/Al_2O_3 (N) catalyst displayed a significantly different NO profile from that observed on the Pd/Al_2O_3 (Cl) (Fig. 8b). The NO signal was characterized by a peak at 534 K and a shoulder at 650 K. This difference could be due to the palladium dispersion, since the higher NO dissociation was observed on the less dispersed Pd/Al_2O_3 (N) catalyst. The modification of the alumina surface could be ruled out, since both catalysts presented similar IR spectra of NO adsorption on alumina. However, as on the Pd/Al_2O_3 (Cl) catalyst, the amount of desorbed NO was still high (Table 5). On the other hand, the N_2 and N_2O profiles were similar to those observed in Fig. 8a.

Figures 8c and 8d illustrate the TPD spectra obtained following NO adsorption over $Pd–Mo/Al_2O_3$ (Cl) and $Pd–Mo/Al_2O_3$ (N) catalysts, respectively. Noteworthy is that only small amounts of NO were observed in the presence of MoO_3, which suggested that adsorbed NO underwent extensive decomposition during TPD. The primary nitrogen-containing species observed were N_2 and N_2O (Table 5). It is important to stress that TPD spectra of NO on the

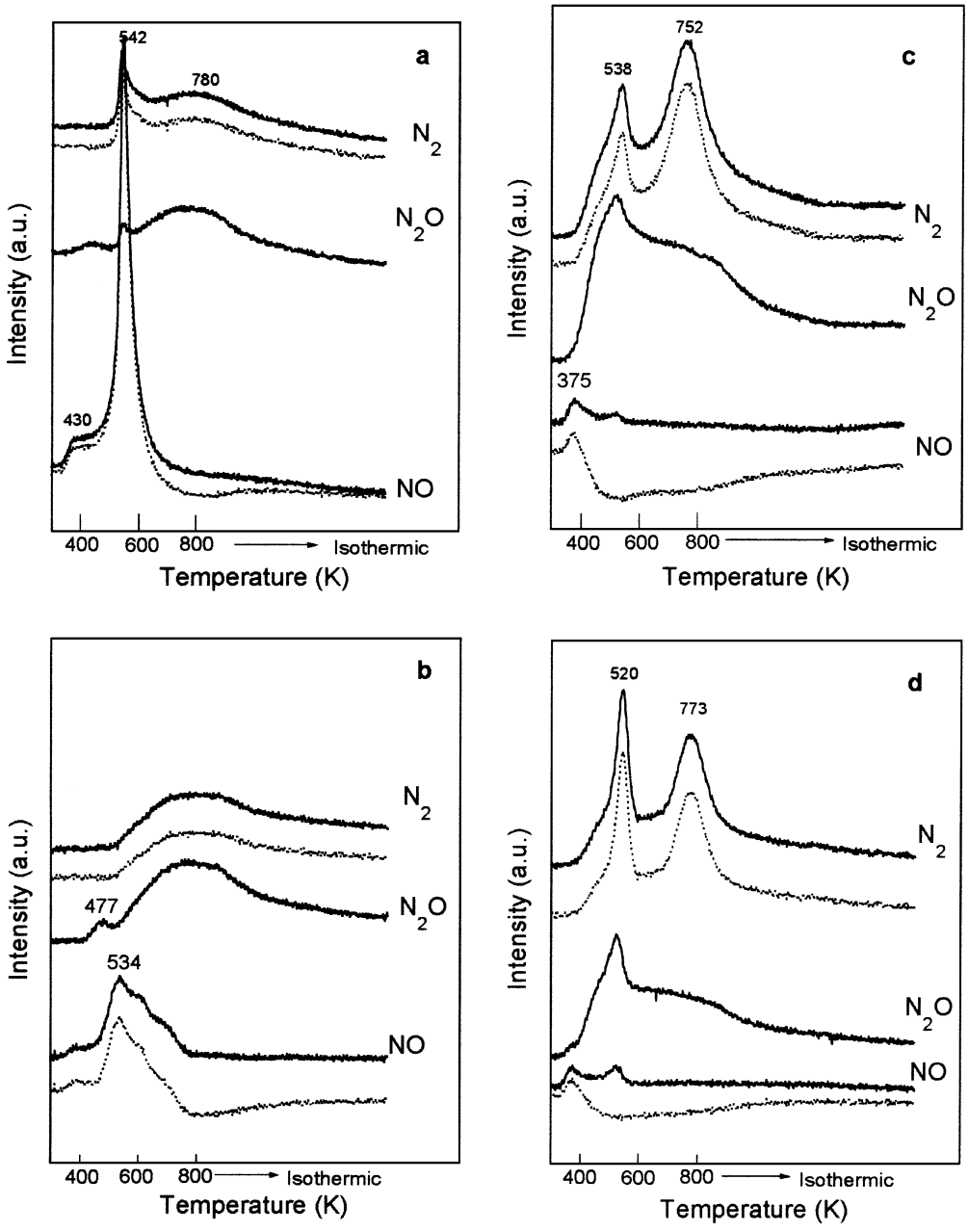

FIG. 8. TPD spectra of NO adsorbed on (a) Pd/Al_2O_3 (Cl), (b) Pd/Al_2O_3 (N), (c) $Pd–Mo/Al_2O_3$ (Cl), and (d) $Pd–Mo/Al_2O_3$ (N). Dashed lines correspond to corrected spectra.

Mo/Al_2O_3 catalyst exhibited a small peak of N_2 at around 500 K.

Cordatos and Gorte studied the adsorption properties for CO and NO on ceria-supported Pd model catalysts (31). Their TPD results indicated that the presence of ceria could significantly enhance NO dissociation. Rao *et al.* (32) also reported evidence for NO dissociation over reduced ceria-containing catalysts. The Ce^{4+}/Ce^{3+} redox couple promoted NO reduction over the Ce^{3+} sites to give N_2 and N_2O. Praliaud *et al.* (33) proposed a bifunctionnal mechanism for the reduction of NO on ZrO_2-supported Pd catalysts. According to them, the oxygen vacancies created on the support by CO adsorption on Pd were directly involved in the NO dissociation. In this case, the active sites would be located at the metal–support interface.

In our work, TPR and IR measurements of CO or NO adsorption revealed the presence of molybdenum oxide partially reduced on Mo/Al_2O_3 and $Pd\text{-}Mo/Al_2O_3$ catalysts. In addition, the TPD spectrum of adsorbed NO on the Mo/Al_2O_3 catalyst provided evidence for NO dissociation

over these molybdenum oxides partially reduced. In fact, palladium catalyzed the reduction of molybdenum oxide on $Pd–Mo/Al_2O_3$ catalysts, as suggested by TPR and IR analysis. Then, the enhancement of NO dissociation to produce N_2 and N_2O on the Pd–Mo catalysts was directly related to the higher amount of reduced molybdenum, as proposed for CeO_2 and ZrO_2.

In addition, the Pd/Al_2O_3 (N) and the $Pd–Mo/Al_2O_3$ (N) catalysts presented completely different yields toward N_2 and N_2O, although having the same dispersion (Table 5). Therefore, a particle size dependence on the selectivities could be ruled out.

Furthermore, two N_2 desorption peaks were observed on the TPD spectra of NO on the Pd–Mo catalysts. A desorption peak at low temperature was noted at 538 and 520 K and a peak at high temperature appeared at 752 and 773 K on $Pd–Mo/Al_2O_3$ (Cl) and $Pd–Mo/Al_2O_3$ (N) catalysts, respectively. On the other hand, only one peak at 780 K was observed on the Pd/Al_2O_3 catalyst.

The TPD spectra of NO adsorbed on the Pd(111) and Pd(100) surfaces and Pd/Al_2O_3 catalysts also showed two N_2 desorption peaks, which were attributed to the atomic nitrogen (34, 35). According to Goodman's group (34, 35), the peak at high temperature corresponds to inactive adsorbed nitrogen species, which are more strongly bounded. These N_a species inhibited further NO adsorption and dissociation.

By comparison of the N_2 signal on the TPD spectra of NO adsorbed on Pd/Al_2O_3 and $Pd–Mo/Al_2O_3$ catalysts, it can be seen that the addition of molybdenum oxide decreased the fraction of the inactive N_a species. In fact, adsorbed nitrogen was more weakly bonded to the molybdenum oxide partially reduced than on the palladium surface. This could explain the higher dissociation of NO toward N_2 and N_2O on the Pd–Mo catalysts. On the other hand, the enhancement of NO reduction could also be explained through a modification of the electronic properties of the palladium in the presence of the molybdenum oxide partially reduced. The IR measurements showed that the MoO_3 addition decreased the adsorption strength of CO on Pd. Therefore, the formation of new adsorption sites between palladium and molybdenum oxide partially reduced could decrease the stabilization of atomic nitrogen on the surface of palladium, promoting the NO dissociation.

The selectivities of the Pd and Pd–Mo catalysts for the $NO + CO$ reaction are shown in Table 6. The addition of MoO_3 increased the selectivity toward N_2, mainly on the catalyst prepared from the nitrate precursor. Gandhi *et al.* (4) and Halasz *et al.* (5) obtained the same results. According to Halasz *et al.* (5), the high $N_2 + N_2O$ selectivity was due to the molybdena contribution to the high-temperature catalytic properties of the $Pd–Mo/Al_2O_3$ under oxygen-free conditions.

TABLE 6

NO Conversion and Selectivity toward N_2 in an $NO + CO$ Reaction at 493 K

Catalyst	NO conversion (%)[a]	N_2 selectivity (%)
Pd/Al_2O_3 (Cl)	18	12
Pd/Al_2O_3 (N)	8	0
$Pd–Mo/Al_2O_3$ (Cl)	12	26
$Pd–Mo/Al_2O_3$ (N)	10	100

[a] NO conversion at 493 K.

As proposed in the literature for CeO_2-supported (32) and ZrO_2-supported (33) Pd catalysts, a bifunctional mechanism could be suggested to explain the catalytic behavior of $Pd–Mo/Al_2O_3$ catalysts.

Our TPD and catalytic results clearly showed an important role of the molybdenum oxide on the promotion of NO reduction to give N_2 and N_2O. The molybdenum oxide promoted the NO dissociation through the formation of oxygen vacancies in the presence of palladium. The CO adsorbed on the Pd surface could react with oxygen to form CO_2.

In contrast to our TPD results, the $Pd–Mo/Al_2O_3$ (N) catalyst exhibited a higher N_2 selectivity in the $CO + NO$ reaction than the $Pd–Mo/Al_2O_3$ (Cl) catalyst. However, this result was related to the presence of a high amount of molybdenum oxide partially reduced, as revealed by TPR. This apparent discordance could be explained by the simultaneous presence of CO and NO on the catalytic test, which confirmed the bifunctional mechanism proposed with the Pd–Mo catalysts.

CONCLUSIONS

The addition of 8 wt% molybdenum covered the surface of alumina and led to the disappearance of the surface hydroxyls. This was evidenced by the suppression of the water–gas shift reaction during the TPD of CO. Furthermore, the bands corresponding to the adsorption of NO on alumina disappeared on the $Pd–Mo/Al_2O_3$ (Cl) catalyst. However, the bands associated with the NO adsorption on alumina increased on the $Pd–Mo/Al_2O_3$ (N) catalyst due to the modification of the Mo/Al_2O_3 precursor during impregnation with the palladium nitrate solution. These results explained the lower NO yield observed on the TPD of NO adsorbed on $Pd–Mo/Al_2O_3$ (Cl) than on the catalyst prepared from the nitrate precursor.

The MoO_3 addition also induced modfications on the metallic phase. On the $Pd–Mo/Al_2O_3$ (Cl) catalyst, the following were observed: (i) a decrease in the amount of hydrogen adsorption; (ii) an increase in the linear/bridged CO ratio, and (iii) the disappearence of the NO adsorption band on Pd. These results suggested the dilution or blocking of

the palladium surface by molybdenum oxide species. Only the reduction of the hydrogen adsorption capacity occurred on the Pd–Mo/Al_2O_3 (N) catalyst, probably due to low dispersion.

TPR and IR analyses of CO or NO adsorption revealed that palladium addition promoted the reduction of molybdenum oxide. The presence of a higher amount of molybdenum oxide partially reduced improved the NO dissociation to N_2 and N_2O on Pd–Mo/Al_2O_3 catalysts. It could be attributed to a lower fraction of inactive adsorbed nitrogen species on molybdenum oxide partially reduced. The catalytic behavior of the Pd–Mo/Al_2O_3 catalysts on the NO + CO reaction could be explained by a bifunctional mechanism. After adsorption and dissociation of NO on Mo^{4+}, the oxygen dissociated is transferred to the Pd. The CO adsorbed on the Pd surface reacts with CO_2. As demonstrated by TPR, the Pd–Mo/Al_2O_3 (N) catalyst presented a higher amount of molybdenum oxide partially reduced than the Pd–Mo/Al_2O_3 (Cl) catalyst. These results are in agreement with the proposed mechanism.

REFERENCES

1. Taylor, K. C., *Catal. Rev. Sci. Eng.* **35**, 457 (1993).
2. Kobylinski, T. P., and Taylor, B. W., *J. Catal.* **33**, 376 (1974).
3. Adams, K. M., and Gandhi, H. S., *Ind. Eng. Chem. Prod. Res. Dev.* **22**, 207 (1983).
4. Ghandi, H. S., Yao, H. C., and Stepien, H. K., *in* "Catalysis Under Transient Conditions" (A. T. Bell and L. L. Hegedus, Eds.), ACS Symposium Series, Vol. 178, p. 143. ACS: Washington, DC, 1982.
5. Halasz, I., Brenner, A., Shelef, M., and Simon, Ng., *Appl. Catal. A* **82**, 51 (1992).
6. Halasz, I., Brenner, A., and Shelef, M., *Appl. Catal. B* **2**, 131 (1993).
7. Hoost, T. E., Graham, G. W., Shelef, M., Alexeev, O., and Gates, B. C., *Catal. Lett.* 57 (1996).
8. Miguel, A. H., and Andrade, J. B., *J. Bras. Chem. Soc.* **1**, 124 (1990).
9. Noronha, F. B., Primet, M., Frety, R., and Schmal, M., *Appl. Catal.* **78**, 125 (1991).
10. Benson, J. E., Hwang, H. S., and Boudart, M., *J. Catal.* **30**, 46 (1973).
11. Rakai, A., Tessier, D., and Bozon-Verduraz, F., *New J. Chem.* **16**, 869 (1992).
12. Chung, K. S., and Massoth, F. E., *J. Catal.* **64**, 320 (1980).
13. Chen, G., Chou, W. T., and Yeh, C. T., *Appl. Catal.* **8**, 389 (1983).
14. Chang, T. C., Chen, J. J., and Yeh, C. T., *J. Catal.* **96**, 51 (1985).
15. Yao, H. C., *Appl. Surf. Sci.* **19**, 398 (1984).
16. Willians, C. C., and Ekerdt, J. G., *J. Phys. Chem.* **95**, 8791 (1991).
17. Cordero, R. L., Gil-Lambias, F. J., and López-Agudo, A., *Appl. Catal.* **74**, 125 (1991).
18. Eischens, R. P., Francis, S. A., and Pliskin, W. A., *J. Phys. Chem.* **60**, 194 (1956)
19. Vannice, M. A., and Wang, S. Y., *J. Phys. Chem.* **85**, 2543 (1981).
20. Soma-Noto, Y., and Sachtler, W. M. H., *J. Catal.* **32**, 315 (1974).
21. Kugler, E. L., and Boudart, M., *J. Catal.* **59**, 201 (1979).
22. Hicks, R. F., Yen, Q. J., and Bell, A. T., *J. Catal.* **89**, 498 (1984).
23. Rieck, J. S., and Bell, A. T., *J. Catal.* **96**, 88 (1985).
24. Rieck, J. S., and Bell, A.T., *J.Catal.* **99**, 262 (1986).
25. Rieck, J. S., and Bell, A. T., *J. Catal.* **103**, 46 (1987).
26. Jackson, S. D., Glanville, B. M., Willis, J., and Whyman, R., *J. Catal.* **139**, 207 (1993).
27. Baldanza, M. A. S., Vannice, A., and Schmal, M., submitted for publication.
28. Hoost, T. E., Otto, K., and Laframboise, K. A., *J. Catal.* **155**, 303 (1995).
29. Solymosi, F., and Rasko, J., *J. Catal.* **62**, 253 (1980).
30. Peri, J. B., *in* "Catalysis Science and Technology," Vol. 5, p. 207, 1984.
31. Cordatos, H., and Gorte, R. J., *J. Catal.* **159**, 112 (1996).
32. Rao, G. R., Fornasiero, P., Di Monte, R., Kaspar, J., Vlaic, G., Balducci, G., Meriani, S., Gubitosa, G., Cremona, A., and Graziani, M., *J. Catal.* **162**, 1 (1996).
33. Praliaud, H., Lemaire, A., Massardier, J., Prigent, M., and Mabilon, *Stud. Surf. Sci. Catal.* **101**, 345 (1996).
34. Vesecky, S. M., Rainer, D. R., and Goodman, D. W., *J. Vac. Sci. Technol. A* **14**, 1457 (1996).
35. Rainer, D. R., Vesecky, S. M., Koranne, M., Oh, W. S., and Goodman, D. W., *J. Catal.* **167**, 234 (1997).